# Tests with a Sensitive Specimen Geometry confirm solid elements when the Aspect Ratio is below four

T. Tryland

SINTEF Raufoss Manufacturing AS, Raufoss, Norway

## 1 Background

The 64 km/h frontal offset test is run with a deformable barrier, and the first numerical model of this barrier was made with solid elements to represent the honeycomb blocks. This required development of a special element formulation to handle the severe deformation of the solid elements together with a complex material model to handle the extreme anisotropy [1]. It is herein important to notice the amount of calibration work as well as the uncertainties with the test specimens and the test procedure to get a proper representation of the honeycomb material. It was therefore suggested to represent the barrier geometry with shell elements that were able to capture the deformation mode with local and global buckling of the honeycomb structure together with a simple model to represent the material in the 0.076 mm thick aluminium foil [2]. Effective learning based on finite element simulations requires that the numerical predictions represent the physics at a relevant level of discretisation. Here simple hand calculations following general structural rules like for example Eurocode may support the user to build a reasonable expectation of how the structure will deform. It is crucial that the numerical prediction captures the correct strain- and stress fields as input when representing the material behaviour until an eventual fracture [3]. One benefit when using a combination of element type and element mesh that predict the correct deformation mode is the simplest possible material model.

The development of computational power has changed the car models since a "complete" model of VW Polo was run into a flat rigid barrier. The 6000 elements had to be fast in 1986, and it was clear that this numerical prediction would improve with smaller elements to represents the relevant parts, see figure 1. Finite element simulations have contributed significantly to passive safety compared with the situation before the 64 km/h frontal offset test was introduced in 1995. It has been possible to run more complex models with reduced element size, and the car models have become significantly more detailed than the full vehicle example illustrated herein [4]. The **KEYWORD** format is extended to open for car models with more than 100 000 000 elements. This means element size about 0.7 mm as a car is made of about 50 square metres with plates. The predicted deformation mode looks realistic as the graphics display smooth surfaces. However, there is limits of shell-discretized structures that are violated especially if localization, damage and rupture are regarded [5]. Developing new software is a large research burden, especially if the problems involve large deformations, nonlinear materials, and contact. Contact treatment for higher order element surfaces is implemented in LS-Dyna. There is ongoing development on a 10-node tetrahedron, and it is likely that a higher order hexahedron is the next. It is relevant to investigate whether increased accuracy and user-friendliness should be prioritised within the best use of numerical power. Main objective here was to present an experimental investigation that confirm the suggested element/mesh rules presented two years ago [6]. Note that these tests were performed with a sensitive specimen geometry to challenge the finite element codes. The tests demonstrate that adjustments in the boundary conditions govern which one out of three different deformation modes that develop within 3% variation in peak force. This means each node in a finite element model of this component has to be represented by correct stiffness to move in space to predict the instability that results in the relevant mode one among these.


*Fig.1: Increased computational power has resulted in FEM models with more elements and details.*

## 2 Effective learning based on FEM

The idea herein is elements that handle the deformation mode at the relevant level of detailing and a material model that handle the properties in a metallic material that have a metallurgical explanation. It is likely that a split like this will improve the learning effect as it reduces the amount of curve fitting of parameters without a direct link to physical phenomenon. The individual focus in the learning process is important to obtain maximum benefit from the four stages [7]. Figure 2 illustrates this by an example where instability is demonstrated with an A4 paper that requires a geometry with sufficient stiffness to utilise the material strength.

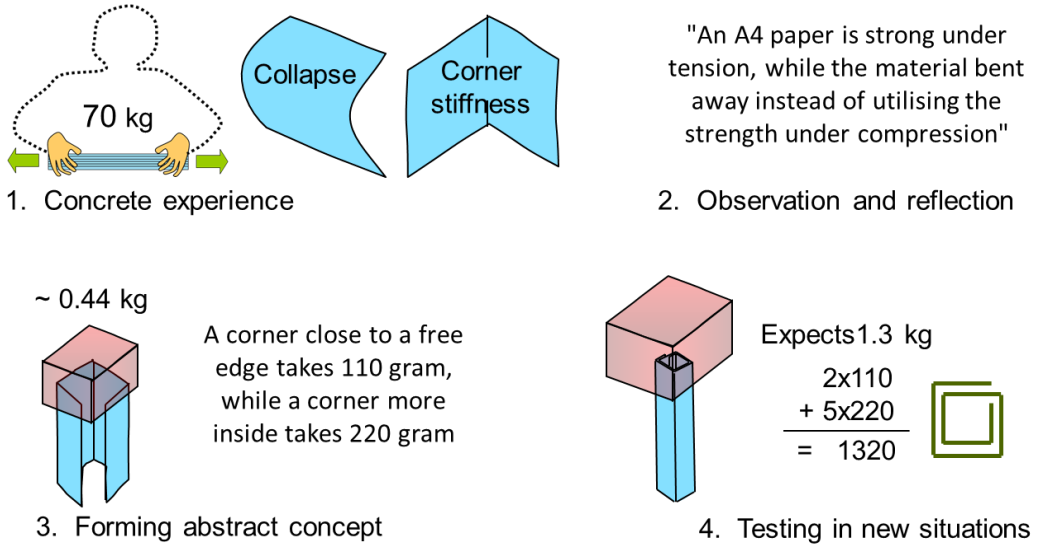


*Fig.2: Illustration of effective learning with an example that show instability of an A4 paper tower.*

Figure 3 demonstrates how experience with an A4 paper model may support the training required to detect the modelling mistake in a new situation based on proper understanding of a uniaxial tensile test. Avoiding misleading results is crucial for effective learning based on FEM, and the key element in this example is to detect the modelling mistake where the numerical connection between the nodes around the hole adds sufficiently stiffness to avoid tear-out at the ends. It worth to remember that the lowest mode is always detected in the real world independent of whether this mode is found in the numerical model, and the costs may be high when the mistake is detected too late.

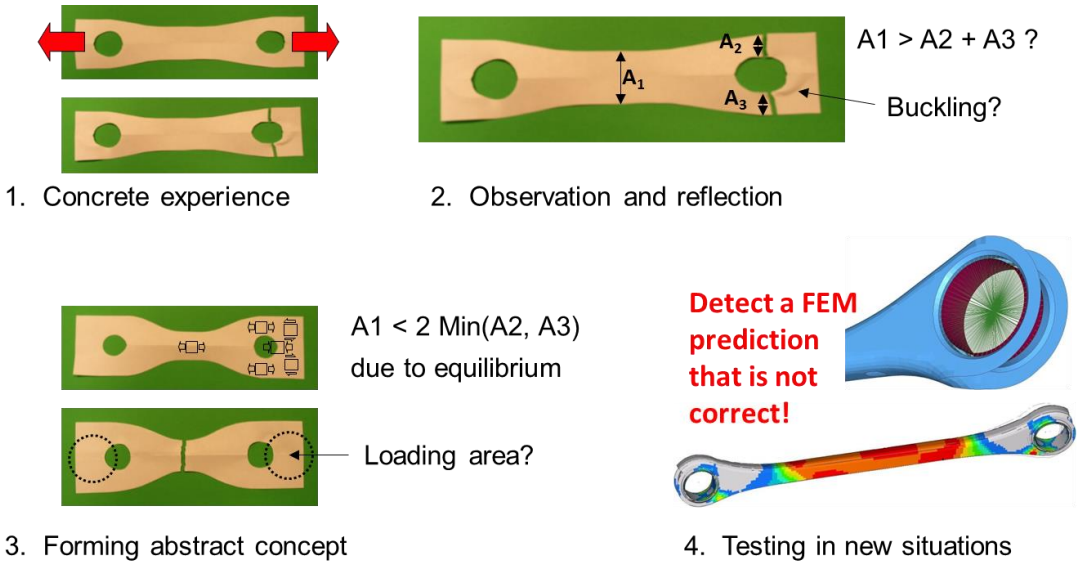


*Fig.3: Effective learning to obtain realistic expectations before making a new FEM model.*

## 3 A sensitive specimen geometry that may challenge the elements

Interactive use of finite element simulations and testing is likely to result in learning that is more effective. The starting point herein was a classification chart based on axial compression of circular aluminium tubes with different diameter/thickness-ratio and varying length relative to the diameter [8]. Focus here, as indicated by the lines in figure 4, was to describe how the specimen geometry seems to govern the deformation mode. Tubes with length above 8 times the diameter show global buckling, while the shortest ones show local buckling in the form of concertina rings. Note that tubes with intermediate length show some concertina rings before transition into 2-lobe buckling. The latter mode has some areas where bending to make the fold will follow the borders of elements oriented along the tube and other areas where this will follow the elements rotated 45 degrees. Therefore, to be able to investigate whether the predicted folding mode is independent of element orientation, the numerical model had two variants with 0° and 45° element orientation relative to the length direction. The result was some suggested element/mesh rules presented two years ago [6] where shell elements with aspect ratio above four is recommended to practical engineers, and solid elements with **ELFORM = ÷2** [9] are recommended when the ambition is smaller elements to capture a more local deformation mode. It is worth to notice that a numerical representation of a circular tube with rotated elements relative to the length direction requires some triangular/pentahedron elements at the tube ends, while the same idea for a squared tube requires this type elements towards the corners. It is possible to replace these triangular/pentahedron elements with smaller squared/hexahedron ones, but this is likely to represent some uncertainty compared with a regular mesh based on squared/hexahedron elements. A study that aims to produce experimental results as base for evaluating improved element formulations should be performed with circular tubes to open for the best element mesh in the middle part of the specimen where local and global instability interact to form the deformation mode.

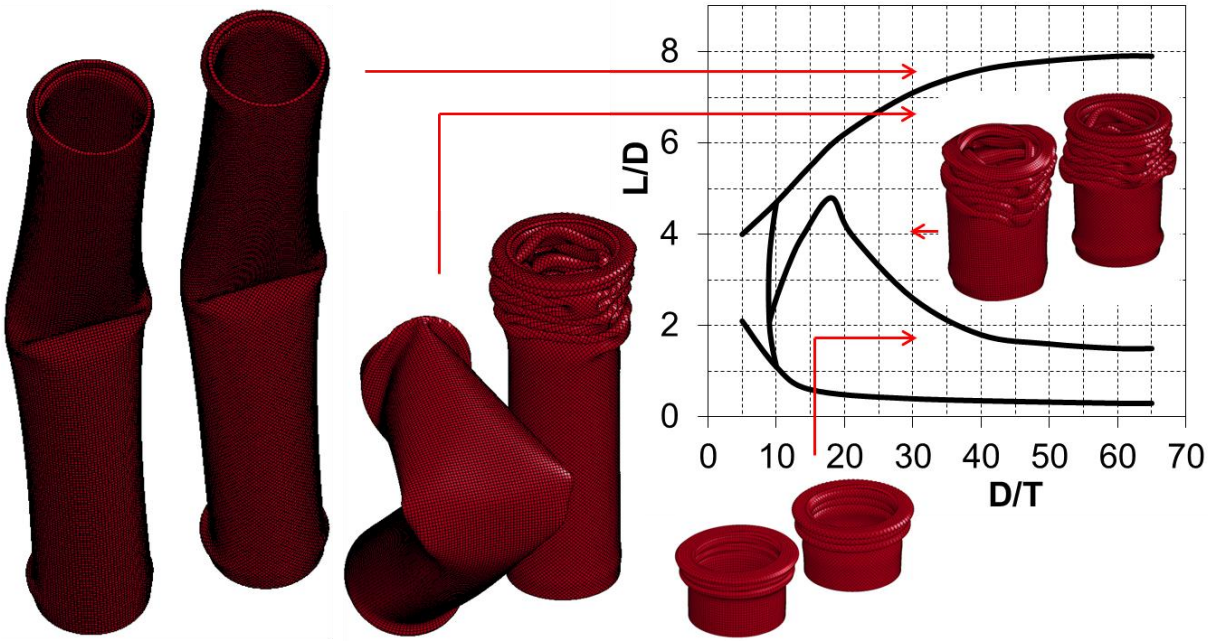


*Fig.4: Initial study to define tests with a sensitive specimen geometry that challenge the FEM codes.*

Both the experimental work by N. Jones [8] and the numerical study presented two years ago [6] seems to indicate a tube with length, diameter and thickness defined by L=6D=180T as a sensitive geometry that has potential to challenge the element formulations. Note that this correspond to one point on a line D=30T in the classification chart in figure 4 where the results with tube length in the range 6D – 8D shows different folding modes that seems to be related to the initial imperfections [6]. Interesting results can be found also at the line D=45T or at other areas in the chart where the deformation mode is a result of interaction between local and global instability. In this case, the diameter was chosen about 30 times the thickness to get a cross-section with sufficiently high slenderness to get local instability modes and at the same time have relatively thick walls that can be represented numerically by either solid or shell elements. The question is whether it is possible to control the experimental uncertainties and get tests results that define the correct deformation mode.

## 4 Measurements of geometrical imperfections

The profile with nominal diameter 63.0 mm and nominal thickness 2.0 mm were delivered in lengths about 2000 mm where the initial straightness deviation was measured with amplitude 0.34 ± 0.13 mm. Here it is worth to notice that the largest value was found somewhere in the mid-area indicating that this is not a simple straightness deviation with radius about 1470 meter. The profile cross-section also shows some ovaling that influenced the measurements of the initial bend, and it was challenging to find some trends in this variation of small values relative to the accuracy of the measurement device.

However, a line that was visible along the profile defined the orientation 0°, and the most prominent variations was determined by analysis of variance. Figure 5 presents the mean values and standard deviations for some geometrical imperfections where the different modes are illustrated with 10-100x amplitudes. Herein it is worth to notice that the four imperfection modes at right hand side is one likely split of the thickness measurements 1.91 ± 0.02 mm and the diameter variation 63.02 ± 0.09 mm. The smallest wall thickness was found in the segment 0° - 45°, while the thickest area was 225° – 270°. It should also be noticed that the illustration of the random variation might be questionable as it consists of both uncertainties from the thickness measurements itself and some thinner and thicker ones among the delivered 2 meter lengths that was not identified and varied systematically to evaluate this effect during the test program. It is also worth to notice the straightness deviation that is a maximum value for the length 384 mm since this value was detected for one of these specimens while the others had a lower amplitude. Finally, the 3-lobe ovaling in figure 5 has to be seen as one possibility whereas the measurements could not exclude the presence of for example 2-lobe and 4-lobe ovaling as well. However, the amplitudes had to be small, and an important part of this study was to define a test arrangement that could overcome these experimental uncertainties.

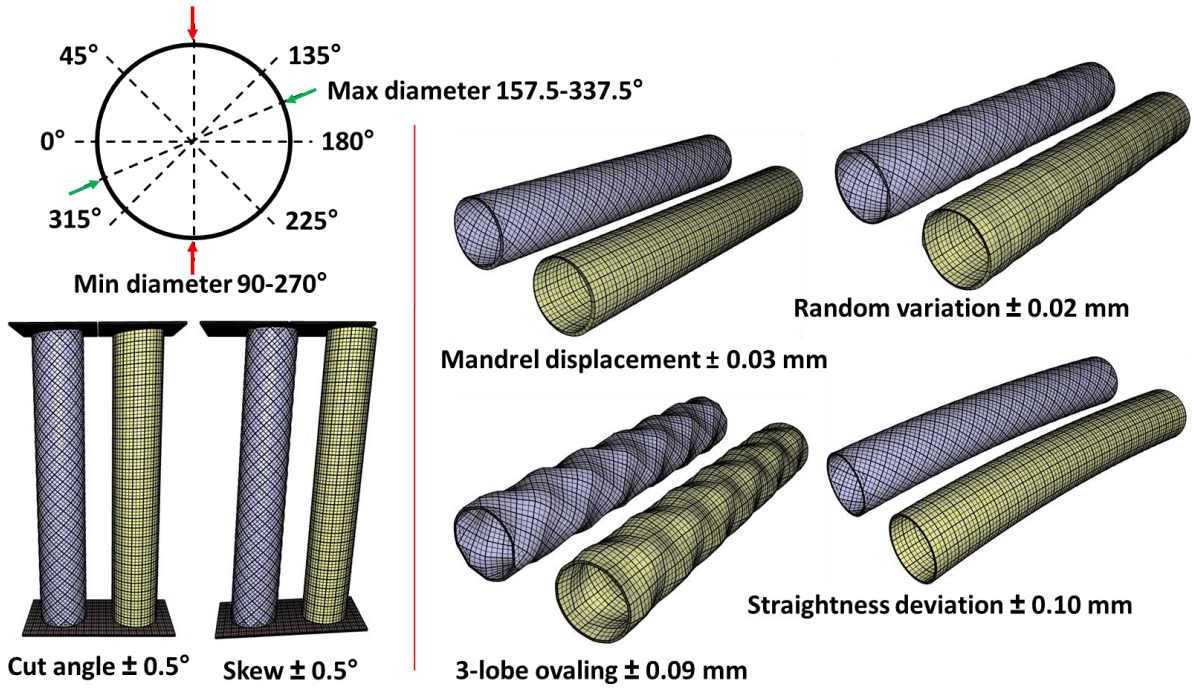


*Fig.5: Measured imperfections with reference to length, diameter and thickness L=6D=180T.*

Some of the test specimen was cut with an angle 0.5° at one end, and this is shown at left hand side in figure 5. Moreover, there is a risk that the upper and lower table in the quasi-static presses were not perfect horizontal leading to specimens that deviate from perfect vertical.

The figure above also illustrates the idea with two mesh variants where the elements are oriented with the angles 0° and 45° relative to the length direction to evaluate whether this influences the predicted response. The initial geometry of a circular tube is simple and can be represented by a relatively coarse mesh, but this is likely to change when the tube is subjected to axial folding. The deformation starts to localise, and a refined mesh is required to capture the details. In addition, the imperfection mode denoted 3-lobe ovaling demonstrates that a relatively fine mesh with limited distance between the nodes is required to represent the local geometrical variations.

## 5 Measurements of material properties + defined a geometry to evaluate the material

Uniaxial tensile tests were performed with specimens taken from some of the delivered 2 meter profile lengths, and the variation in yield stress was measured with mean value 191 MPa and standard deviation 6 MPa. Also somewhat variation in strain hardening was observed, and typical curves for true stress vs true strain were correlated with the Voce Law defined with parameters A = 189 ± 6 MPa, Q1 = 47 ± 4 MPa, C1 = 21.5 ± 3.5, Q2 = 100 MPa, C2 = 0.1 and elastic modulus E = 70 000 MPa.

Here it is important to remember that only the first part of the stress-strain curve can be measured directly, while the response after necking is a result of the interaction between geometry and material. Therefore, axial compression of the same profile with length L = 2D was investigated to understand the strain field with severe localisation when one fold get in contact with the previous one. The result was four concertina rings when these specimens were deformed to half of the initial length. Figure 6 shows the deformation mode for the base geometry with diameter about 63 mm, a smaller tube with nominal diameter like 32 mm and a larger one with diameter about 125 mm. The three specimens have close to the same relative dimensions L = 2D = 60T, and they scale as expected due to the scale 0.5X, 1X and 2X where the first one shows about one fourth of the peak force, while the large one shows about four times the peak force. The fact that these specimens show exactly the same deformation mode indicates that the through-thickness material variation is limited. Remember that an eventual surface layer with thickness about 0.2 mm both inside and outside means about 40 % of the thickness for the smallest specimen, about 20 % for the base geometry and close to 10 % for the largest specimen.


*Fig.6: Specimens with L = 2D = 60T shows four concertina rings when compressed into half-length.*

The AA6060 T6 material tested in these circular tubes was not homogeneous. Figure 7 shows two segments that were cut out from the folded region and prepared to display the grain structure. There is a line of grains located at the mid-thickness, and it is clearly shown how the grains are deformed at the side under compression vs the side under tension. In addition, a crack in an area with severe shear stress is visible at right hand side in figure 7.

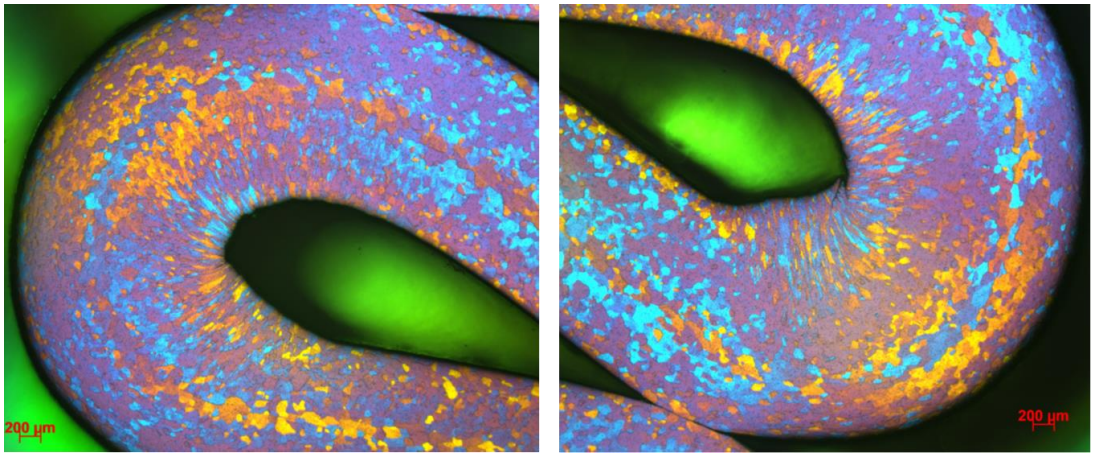


*Fig.7: A cut through the concertina rings show how the grains in the profile wall are deformed.*

## 6 Define specimen geometry and test procedure

The objective was to evaluate axial compression of a circular tube with length, diameter and thickness L = 6D = 180T. This geometry seems to be sensitive with three different deformation modes within 3% variation in peak force. Figure 8 shows five parallel test with this tube geometry where the first four show global buckling, while the last one shows seven concertina rings before transition into 2-lobe buckling. Measured peak force was 68.42 kN, 69.80 kN, 69.56 kN, 73.45 kN and 74.82 kN. This means mean value like 71.2 kN and standard deviation like 2.8 kN. The idea was to measure the thickness and take samples for uniaxial tensile testing from all delivered 2 meter lengths and thereby investigate eventual correlation with variation in peak force. However, the total test program involved many different specimen lengths resulting in everything from one to seven specimens from each delivered profile length. It was therefore not performed a systematic study of thickness and yield stress variations related to the effect on peak force, but it was possible to find the highest yield strength and thickness among the specimens with highest capacity and the lowest values among those with lowest capacity. Therefore, it seems like experimental values corresponds well with about ±3% variation in peak force that has to be expected due to variation in material properties and about ±1% caused by thickness variation.


*Fig.8: Results with the sensitive geometry defined with length, diameter and thickness L = 6D = 180T.*

It was important to define a test procedure that overcome the experimental uncertainties related to geometrical imperfections and local variation in material properties that are hard to measure. Section 5 describes tests with different scales as an indication that an eventual through-thickness yield strength variation has to be small. This means it make sense to use uniaxial test specimens covering the complete wall thickness, and a numerical model can be made with one material model instead of separating it into different layers through the thickness. Alloy 6060 T6 is a relative low strength variant with low content of alloying elements and fully recrystallized. It should not have significant anisotropy [10], but there may be somewhat different properties in tension and compression due to some stretching on the press table. It is likely that these uncertainties will not influence how the profile starts to deform, and an eventual Bauschinger effect is likely to influence the peak force rather than the deformation mode.

In addition comes some variation in peak force caused by the geometrical imperfections. It is recommended to define parameters that can be varied systematically and randomise possible effects where this is not possible [11]. The idea herein was to use a quasi-static press with relatively large

stiffness and a cut angle like 0.5° to introduce some bending in addition to axial compression at the upper end. However, the measured straightness deviation was small, and it is likely that not all parallel specimens, that were oriented to work either together or opposite to the cut angle, were tested in accordance with this intension. This means four blocks in the analysis of variance as the tests with a small press, the tests with no cut angle and the tests with increased friction were varied systematically, while positive and negative straightness deviation relative to the effect of cut angle could not be separated from each other. The result was most of the profiles initiated with cut angle 0.5° at the upper end show global buckling, and the fact that this took place somewhat above the mid-height indicated lower support from this end. Exactly where this took place was influenced by how the local and global imperfections interacted, and figure 9 illustrates how this was measured to determine this variation. Section 7 presents a more comprehensive description of how this also influenced the details in the deformation mode.

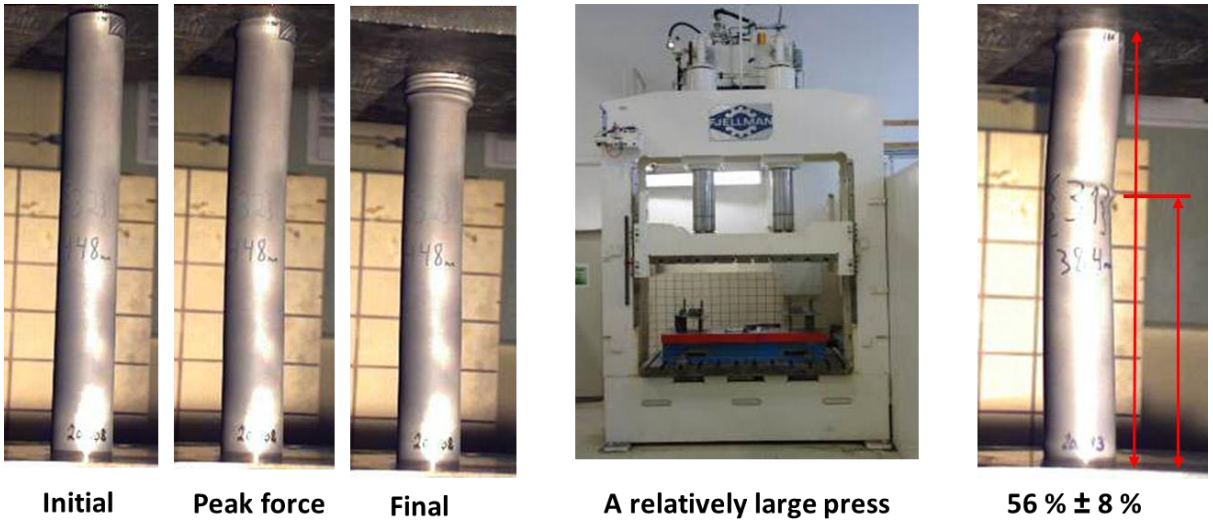


*Fig.9: Most profiles with cut angle 0.5° show global buckling somewhat above mid-height.*

Figure 9 also illustrates the relatively large quasi-static press that was instrumented with proper sized loadcells spread out under the lower table to keep the high stiffness. In addition, three pictures from one test movie are included to show one profile where the cut angle 0.5° seems to initiate global buckling before the upper end reach its limit and starts to deform into a concertina mode.

## 7 Experimental results showing parallel tests at different lengths

This experimental study was based on circular aluminium tubes with diameter to thickness ratio about 30 that means sufficient cross-section stiffness to reach the yield stress when the tested tube was short, see figure 10. The length was then increased from initial L = 2D to L = 4D, and both show four concertina rings when the tubes was compressed into 1D reduction in length. This figure also shows global buckling for the tested tubes with lengths 6D, 7D, 7.5D, 8D, 8.5D, 9D, 12D, 15D, 19D and 23D. All these tests were performed with diameter D = 63.02 ± 0.09 mm, and the tested specimens are presented in figure 10, but unfortunately the cutting length refer to 64 mm as base length for D.

The tubes with the highest column slenderness had lengths 1301 mm and 1996 mm. They are not presented with the tested specimens in figure 10, but the variation in peak force is included as two vertical lines at right hand side. Here it is worth to notice that a smaller profile with nominal diameter 32 mm was used to reach 41D and 62D inside the delivered 2 meter profile lengths, and real dimensions with ovaling inside $31.77 < D < 32.10$ mm and thickness variation $1.02 < T < 1.05$ mm were measured for this profile. The measured peak force for these tests shows that the buckling length factor K = 0.7 from table 6.8 in Eurocode 9 [12] for columns held in position and restrained in direction at both ends are conservative. The Euler curve defines an upper limit, and it seems likely that a press with relatively high stiffness is able to support the tube sufficiently to reduce the buckling length to half of the distance between the upper and lower table. Remember that for columns held in position at both ends the relative stiffness to prevent also rotation of the ends determine the buckling length factor in the range $0.5 \leq K \leq 1$.

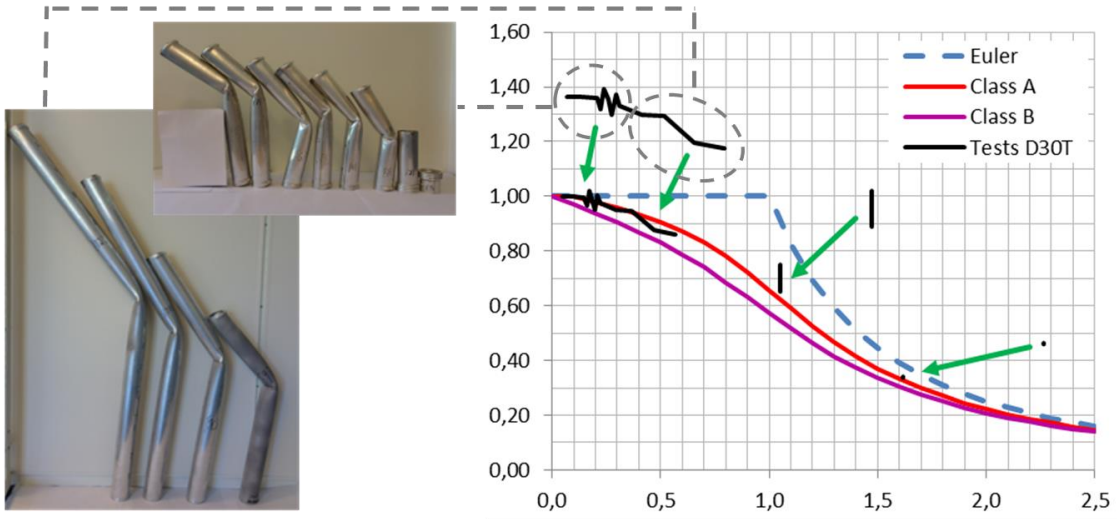


*Fig.10: The tests show higher yield stress and reduced buckling length compared with Eurocode 9.*

The effect of reduced buckling length factor from K = 0.7 to K = 0.5 is illustrated at right hand side in figure 10 where the green arrows moves the test results to the left while higher yield stress than the tabulated value 140 MPa for 6060 T6 gives a component downwards as well. The measured peak force as a result of the behaviour of the shortest tubes with length L = 2D is dominated by the material properties, and experimental results above an estimate calculated by the formulas in Eurocode 9 [12] is a direct result of yield stress above the minimum values defined in this code. Note that the arrows in figure 10 is meant to illustrate the conservatism between measured peak force where the upper line indicates the experimental variation, while the corresponding lower line is based on Eurocode 9 design values. This means yield stress 140 MPa and K = 0.7 instead of more realistic yield stress like 191 MPa in this case and K = 0.5 due to the relatively large press. It is also worth to notice that the tests with length about 41D, which correspond to the vertical line at column slenderness about 1 where the effect from geometrical imperfections is most prominent, are somewhat above both curve A and B.

Circular tubes with lengths 8D are expected to show global buckling, and the specimens shorter than 5D are expected to show local buckling modes starting with concertina rings. It is likely that the profile length about 6D is most sensitive with respect to how the geometrical imperfections influence the deformation mode. This region was therefore investigated with 5 parallels to evaluate whether it was possible to overcome this variation in deformation mode. Figure 11 shows global buckling with specimen length 6D and 6.5D for all tests with the large press, while corresponding tests identified here by a red dot for the small press show local folding.


*Fig.11: Five parallel tests that show the deformation mode for different length 5D < L < 7.5.D.*

It is also worth to notice that all tubes with length 7.5D presented in figure 11 show global buckling, and as presented in figure 10, even longer tubes will bend away into a global mode due to lack of stiffness instead of utilising the material strength.

Figure 12 illustrates the results with different tube lengths. Here are details that may challenge the practical engineers to test out whether their codes are able to predict the correct mode. Developers of new elements should look into figure 7 as well. The column slenderness is increased from the starting point with length L = 2D which shows four concertina rings when the tube is compressed to half of this length into the sensitive range 5D ≤ L ≤ 7.5D where local and global buckling modes interacts. Then follows an intermediate range 8D ≤ L ≤ 15D where the result is a global instability mode that may have some twist as a result of some influence also from the local geometrical imperfections, see figure 12.

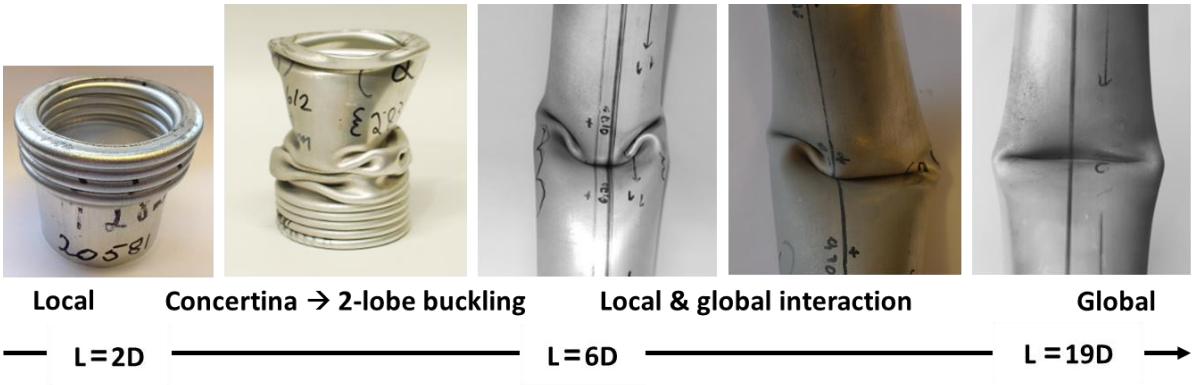


*Fig.12: Tests with details in the deformation mode that may challenge the finite element codes.*

Global buckling dominates when the tubes are even longer, and the largest effect from the straightness deviation is likely for tube lengths about 40D, see figure 10. Here it is crucial to remember the reduced buckling length factor K = 0.5 due to the large press with sufficient stiffness to prevent rotation at the tube ends. An alternative test arrangement where the tube ends are kept in position but free to rotate corresponds to K = 1 and half of these lengths. There is also examples like a crashbox fixed between the car bumper beam and the rail ends where the buckling length factor is larger than one since it is not likely that this assembly represents sufficient stiffness to keep both ends in position. The results is a crashbox profile that has to be even shorter to secure local folding that absorbs the energy instead of a global mode where the force drops to nearly nothing just after the peak.

Remember that one key element to find a design with aluminium that save weight compared with steel is to understand instability as presented herein and increase the cross-section due to lower density with aluminium. Structural engineers often use hand calculations following for example Eurocode 9 [12] to find a proper starting point and build up expectations to what should be the outcome of eventual finite element simulations to optimise this further. There is a need for improved element formulations that handle instability as well as contact and the large strains required to predict the folding mode when one fold meet the previous one. The idea here is that figure 12 showing four concertina rings when the specimen defined with L = 2D = 60T is compressed to half of this length, 5-7 concertina rings before transition into 2-lobe buckling for the L = 4D = 120T specimen and global buckling for the L = 6D = 180T specimen can challenge the element formulations. Note that the experiments were run with cut angle 0.5° at the upper end. An eventual numerical prediction of these deformation modes should be independent of element orientation and element size. However, it is likely that the practical engineers will prefer an estimate where it is clearly visible that the mesh is coarser than required to reach convergence with respect to element size.

## 8 Scaling effect

Most finite element simulations are run under continuum mechanics. This assumption is questionable and related to the level of discretisation where for example the carbon atoms are organised differently inside a pencil and in a perfect diamond. The example with the deformable barrier from the 64 km/h frontal offset test of a car is mentioned in the introduction to this paper. This challenge the idea with an average continuum at a larger scale where shell elements representing the honeycomb cells may be a better numerical representation than solid elements representing a structure with about 99% air. The

result is a more realistic representation of the barrier stiffness and a simple material model that saves hours with calibration work.

An eventual scaling effect is relevant also for this experimental study where an eventual finite element model of axial compression of a circular tube with dimensions L = 6D = 180T is likely to be independent of the actual component size. Metallic components are often represented numerically without any through-thickness variation, and an eventual deviation from this assumption represents an uncertainty related to proper understanding of what is really tested. Figure 6 shows how an eventual through-thickness effect was evaluated by testing short tubes at different sizes, and the results indicate that an eventual through-thickness effect was not prominent when it comes to stiffness and strength. Other uncertainties are described in section 6. However, it is likely they influences the peak force rather than how the profile starts to deform when cut angle 0.5° and a large press seems to work well.

Figure 13 shows how different scale L = 6D = 180T specimens deform under axial compression. Note that the displacement related to length 384 mm is selected as abscissa, while the measured force related to diameter 63.02 mm and tabulated yield stress in Eurocode 9 [12] defines the ordinate. This means tests with half size specimens in 6060 T6 are presented with two times the displacement and four times the peak force as a result of scaled cross-section area, while specimens in 6082 T6 are corrected by the factor 250/140 for different yield stress as well. The results is a direct comparison of test results from different scaled specimens where it is worth to notice that the stiffness become different for the profile with diameter 100 mm due to higher strength with 6082 T6. It is also important to remember that this scaling does not include a case with reduced thickness to get a certain peak force with 6082 T6 relative to 6060 T6. All test were performed with diameter-to-thickness ratio about 30, and thinner walls gives increased tendency to local buckling because of increased D/T-ratio.

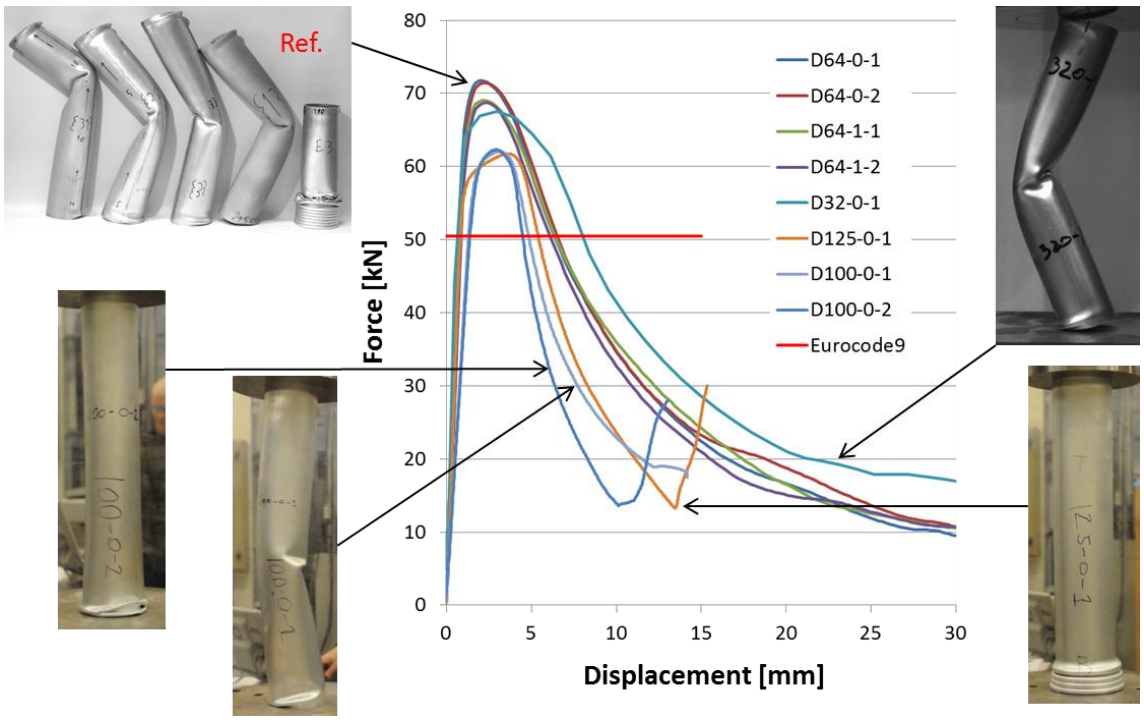


*Fig.13: Scaling effect – does the size of the L = 6D = 180T specimen influence the deformation mode.*

The scaling presented in figure 13 does not contain a high number of experiments, and that has to be taken into account when concluding carefully. The test was performed with four different profiles made with existing extrusion tools. The profiles had diameter 31.8 mm, 63.02 mm, 99.78 mm and 124.7 mm and D/T-ratio in the range 30.3 – 34.5. All tests show peak force well above the values calculated by following Eurocode 9 [12]. The effect of cut angle 0.5° seems not to work with a relatively smaller press, and it seems to be somewhat stronger localisation with larger specimens and higher yield stress. The geometry defined by L = 6D = 180T seems to be sensitive also for other dimensions as two parallel tests with nominal diameter 100 mm gives global buckling as one result and local folding for the other one. Here it is not clear whether it is D/T = 34.5 or higher yield stress with 6082 that determine only one concertina ring before transition into 2-lobe buckling as the local folding mode.

## 9 Discussion and further work

It may be interesting to perform more tests with different size specimens as well as other aluminium alloys to evaluate whether the geometry defined by L = 6D = 180T is sensitive for the 6060 T6 and diameter 64 mm scaled 0.5X, X and 2X only or if this is valid for other materials and scaled geometries as well. Both the cross-section slenderness and the column slenderness are in ranges where the peak force is reached outside the elastic regime, and it is likely that the first part where the stress-strain curve determined from uniaxial tensile tests may have some influence. Remember that the profiles are stretched somewhat on the extrusion press table, and the result may be somewhat different material properties in tension and compression. It could therefore be interesting to test sufficiently large specimens to open for uniaxial tension and compression with short circular specimens machined from the profile wall. This will detect an eventual Bauschinger effect, and an eventual anisotropy will result in ovaling of the deformed cross-section.

The ratio between the elastic modulus and the yield stress may have some influence, and tests with other materials could be of interests. Here it is likely that aluminium and steel will behave similar, while components made of polymer materials could have somewhat reduced length and diameter compared with the wall thickness to compensate for lower elastic modulus relative to the stress at 0.2% plastic strain. Finally, it could be interesting to test composite materials with the geometry defined by length, dimeter and thickness L = 6D = 180T to evaluate whether the matrix material has sufficiently stiffness to effectively support the fibres when the tube wall has to withstand both local and global instability.

Also the geometries defined by L = 2D = 60T and L = 4D = 120T could relevant when testing other materials and scales to determine eventual alternatives to four concertina rings as well as alternative transitions into other modes than those shown in figure 12. Here it is likely that materials with lower elastic modulus relative to the yield stress will deform into 4-lobe or 3-lobe buckling instead of 2-lobe buckling for the 6060 T6 material presented here.

Figure 14 shows how these numerical simulations based on cubic shaped solid elements struggle to predict correct deformation mode with all relevant details, and this indicates there is a need for improved element formulations that represents correct stiffness both for small and large deformations. The challenge here is to find an element formulation that has sufficiently high stiffness with respect to local modes to predict global buckling for L = 6D = 180T and at the same time has sufficiently low stiffness with respect to local modes to predict four concertina rings for L = 2D = 60T compressed to half of this length. Here a sufficiently coarse mesh is the simplest alternative to predict the first one, but the result is likely to be less than four concertina rings for the short one and details that are not captured for the long one as well.

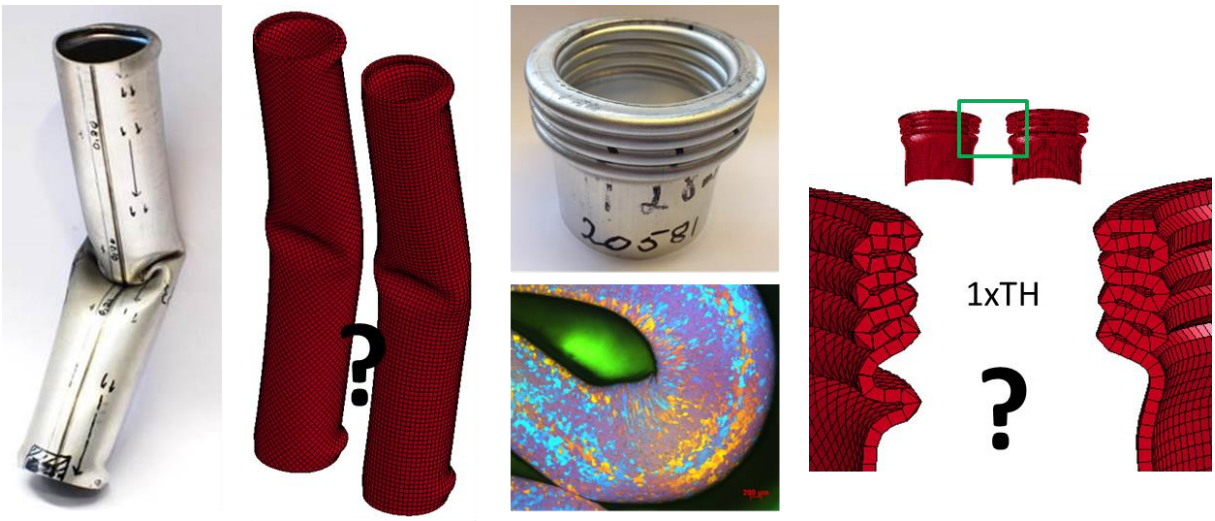


*Fig.14: A numerical model based on cubic shaped solid elements does not predict all relevant details.*

## 10 Acknowledgements

The research within this study was supported by grant 245329/O30 from the Research Council of Norway. The support is gratefully acknowledged.

## 11 Summary

The objective was to presents well-documented experiments that challenge the element formulation both with respect to correct stiffness when predicting instability as well as handle the strain field with severe localisation when one fold get in contact with the previous one. Test results with axial compression of a sensitive tube geometry defined by length, diameter and thickness L = 6D = 180T together with a robust geometry L = 2D = 60T deformed to half of initial length confirms shell elements with aspect ratio above four, while solid elements is recommended when the ambition is smaller elements to capture a more local deformation mode. It is relevant to investigate whether increased accuracy and user-friendliness should be prioritised within the best use of numerical power, and it is likely that the experiments presented here show useful details to verify improved element formulations.

## 12 Literature

[1] Kojima, S., Yasuki, T., Mikutsu, S., Takatsudo, T.: "A Study on Yielding Function of Aluminium Honeycomb", 5th European LS-DYNA Users Conference, Birmingham, UK, 2005.
[2] Tryland, T.: "Alternative Model of the Offset Deformable Barrier", 4th LS-DYNA Forum, Bamberg, Germany, 2005.
[3] Tryland, T., Berstad, T.: "Keep the Material Model simple with input from Elements that predict the Correct Deformation Mode", 10th European LS-DYNA Conference, Würzburg, Germany, 2015.
[4] A free Ford Taurus LS-Dyna model developed 2010-2014 within a founded project of Automotive Simulation Center Stuttgart based on an underlying detailed FE-model from the National Crash Analysis Center at George Washington University, 2001.
[5] Haufe, A et al.: "Predictive Fracture Modelling in Crashworthiness: A Discussion of the Limits of Shell-Discretized Structures", 14th LS-DYNA Forum, Bamberg, Germany, 2016.
[6] Tryland, T.: "Combinations of Meshes and Elements that seems able to Predict the Correct Deformation Mode", 13th LS-DYNA Forum, Bamberg, Germany, 2014.
[7] Colb, D A.: "Experimental Learning", Englewood Cliffs: Prentice Hall, 1984.
[8] Jones, N.: "Structural impact", Cambridge University Press, 1989, Figure 9.32.
[9] Borrvall, T.:"A heuristic attempt to reduce transverse shear locking in fully integrated hexahedra with poor aspect ratio", 7th European LS-DYNA Conference, Salzburg, 2009.
[10] Kokkula, S.:"Bumper beam-longitudinal system subjected to offset impact loading", Doctoral theses at Norwegian University of Science and Technology, 2005.
[11] Box, G.E.P., Hunter, W.G. and Hunter, J.S., Statistics for Experimenters, Jon Wiley Sons, 1978.
[12] Eurocode 9: Design of aluminium structures, Part 1-1: General structural rules, European Committee for Standardisation, prEN 1999-1-1: 2003.